Available online at www.sciencedirect.com

ScienceDirect

Ceramics International 40 (2014) 10803–10816

CERAMICS INTERNATIONAL

www.elsevier.com/locate/ceramint

The combined use of petrographic, chemical and physical techniques to define the technological features of Iberian ceramics from the Canto Tortoso area (Granada, Spain)

Giuseppe Cultrone[a,*], Eduardo Molina[a], Anna Arizzi[b]

[a]Department of Mineralogy and Petrology, Faculty of Sciences, University of Granada, Spain
[b]School of Geography and the Environment, University of Oxford, UK

Received 18 February 2014; received in revised form 4 March 2014; accepted 17 March 2014
Available online 21 March 2014

Abstract

Thirty-two ceramic fragments dating from the Early Iberian Age were collected in Canto Tortoso, an archaeological site located about 100 km from the city of Granada (Spain). The site is on a hill bordered by two rivers, the Fardes and the Guadiana Menor.

The ceramics are divided equally into amphorae and vessels and half of them have black cores. The samples are rich in SiO_2 and Al_2O_3, with varying amounts of CaO, Fe_2O_3, MgO and K_2O. The most common mineral is quartz and almost all the samples have muscovite-type phyllosilicates. Calcite appears as small grains dispersed in the matrix and sometimes also of secondary origin covering the surface of samples or filling the pores. One ceramic was richer in calcite grains than quartz. An incipient decomposition of this carbonate is detected even at low firing temperatures. Samples fired at high temperatures are characterised by the presence of mullite or gehlenite and/or diopside phases. These silicates are also accompanied by a vitreous phase that increases the interlocking between the particles and changes the morphology of the pores from angular to round. The precipitation of phases of secondary origin on the surface of the ceramics may have minimised the chromatic differences between Ca-rich and Ca-poor samples. The combined use of chemical, petrographic and physical techniques allowed us to estimate the firing temperature of the ceramic samples (most samples were well-fired) and to discover the provenance of the raw material (a clayey material found near a kiln located just 3 km away from the settlement has a mineralogical composition compatible with that of the ceramics).

Keywords: Iberian ceramics; Canto Tortoso; Early Iberian Age; Raw material provenance

1. Introduction

The Iberian people lived in settled communities in the East and South of the Iberian Peninsula from the VII to the end of III century BC when the Romans conquered the region. They shared a number of common features such as language, art, urban planning and religious rituals, while diverging in other typical aspects of a larger, more established state government such as politics and the economy [1].

The settlement of Canto Tortoso belonged to Bastetania, a region of the southern Iberian Peninsula, and the surviving archaeological remains are today located within the municipal borders of Gorafe (Granada, Spain) in an area of 1.4 ha. This site was discovered during archaeological excavations in 1992 and the findings were described in a monographic work [2].

The settlement was founded on a hill with steep sides that overlook the confluence of two rivers, the Guadiana Menor and the Fardes (Fig. 1) and appears to have gone through three different chronological phases: the first settlement located at the eastern end dates from the Early Calcolitic Age; the second about which we have scant information is from the End of the Bronze Age; and the third and most important from the Early Iberian Age covers almost all of the site and contains the only architectural structures identified. These structures include a wall with a perimeter of 840 m, which has collapsed in many places due to the erosion of the hillside. There are also the remains of several rectangular-shaped houses. A path to the

*Corresponding author.
E-mail address: cultrone@ugr.es (G. Cultrone).

http://dx.doi.org/10.1016/j.ceramint.2014.03.072
0272-8842/

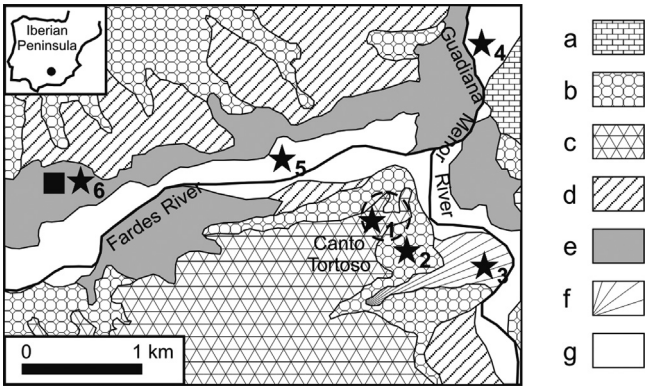

Fig. 1. Geological map of the Canto Tortoso area (Granada, Spain): (a) bioclastic limestones from the Turolian Age; (b) grey, white and ochre clays with levels of conglomerates, silts and carbonates from the Upper Turolian-Pliocene Age; (c) salmon-red clays with conglomerates, silts and carbonates from the Plio-Pleistocene Age (Guadix Formation); (d) depositional pediments composed of clayey-silt sediments with dispersed carbonates from the Middle Holocene Age; (e) present day alluvial fans from the Holocene Age; (f) talus cone from the Holocene Age; and (g) floodplain from the Holocene Age. From Roldán García et al. [51], modified. The perimeter of the settlement is marked with a dashed line. Stars followed by numbers 1–6 represent the location of the raw materials (RAW1–RAW6) we collected, while the square indicates the position of the kiln.

fortified area (about 3 m wide which narrows as it approaches the settlement) is still visible and is unique in the archaeological context of other contemporary settlements.

The recovery of Iberian Age ceramic fragments on Canto Tortoso hill suggests that this fortified settlement was a staging post on the trade route between the northern Guadalquivir (*Castulo*) and the coast of Almeria (*Baria*) [3]. The lack of any direct data from the archaeological excavations prevents us from specifying what goods were being traded. Adroher Auroux and López Marcos [4] suggest that wine and salted fish from the coast were exchanged for beer from more inland areas, all products likely to have been transported in amphorae and similar containers.

Although no previous archaeometric studies have been carried out on the ceramics from Canto Tortoso, there is an extensive bibliography dealing with ceramic artifacts from the Iberian Age, which provides compositional, technological and provenance information. As examples, several studies have been conducted on the ceramics discovered in the South [among others, 1,5,6] and North-East of the Iberian peninsula as well as on trade with neighbours [7–9]. Ceramics were one of the most significant elements of Iberian culture [10] and research has shown that potters had acquired a certain degree of skill not only in the manufacture of more elaborate products [1,11], but also in their knowledge of the raw materials. They learned for example how to prevent "lime blowing" in ceramics made with carbonate-rich clays [12], a skill they were perhaps obliged to attain due to the limited choice of raw materials in the area. The use of one type of raw material rather than another was dictated by the position of the settlement since clays tended to be quarried somewhere in the vicinity [13]. Hence, potters had to use forcedly local clays to make different types of products by varying the proportion of clay, silt and sand fractions and changing the firing temperature and/or the atmosphere [14].

The purpose of our research was to make an initial mineralogical and textural characterisation of the ceramics from Canto Tortoso, to investigate the provenance and the types of raw materials used in their production and to establish the range of firing temperatures. We began by conducting a petrographic study which we then complemented and completed with a series of physical tests. Given that ceramics can provide an insight into the society that manufactured and used them, an accurate characterisation of these materials can contribute to a better understanding of this ancient period of our history.

2. Materials and methods

2.1. Description of the samples

Thirty-two fragments of amphorae and vessels from the Early Iberian Age (VI century BC) were collected in the archaeological settlement of Canto Tortoso. They were selected after an archaeological survey of a larger group of fragments according to their archaeological significance and function. Macroscopically they are red-brown to pale-yellow coloured (Table 1). However, the original colours of ceramics may have been altered by the long exposure to the environmental conditions in the archaeological site. In some cases, the surface is covered by a discontinuous thin white patina. About half of the ceramics have a black core 2–4 mm thick measured on cross-sections (Table 1). Previous authors have attributed the presence of this dark level, sandwiched between the red (or yellow) surfaces, to the use of too fine ceramic body that have after firing a too fine porous texture [15], and the presence of organic matter or other reducing substances in the raw material [16–18]. In this case the poor oxidation of the core of ceramics caused the incomplete burning of organic matter, which was carbonized, and the reduction of iron compounds [19].

Six clayey materials outcropping in the vicinity of the settlement were collected for comparison with the ceramics in order to identify, if possible, the provenance of the raw materials used by the Iberian potters: two of the clays were found close to the settlement, one of these was from the Upper Turolian-Pliocene Age and the other was from the Guadix Formation from the Plio-Pleistocene Age; one was located in the talus cone just below the settlement and another in the sediments of the Guadiana Menor River; the last two were from the Holocene sediments (alluvial fans and floodplain) in the Fardes River. One of these last two sediments was collected near an Iberian Age kiln situated about 3 km away from the settlement, which is thought to date from the VI century BC (Fig. 1 and Table 1).

2.2. Analytical techniques

Major elements of the ceramic samples were determined by X-ray fluorescence (XRF) on fused Li-tetraborate beads using a Philips MagiX PRO model PW2440 spectrometer with Rh 4 kW tube. Prior to the analysis, 5 g per sample was finely milled in an agate mortar. The white patina, observed on the surface of some samples, was removed before milling. The accuracy of our analytical results was evaluated by comparison

Table 1
List of the studied samples (ceramics and raw materials). Legend of the analytical techniques performed on ceramics: XRF = X-ray fluorescence; PXRD = powder X-ray diffraction; POM = polarised optical microscopy; FESEM = field emission scanning electron microscopy; Hydric = hydric tests (water absorption and drying); and MIP = mercury intrusion porosimetry.

	Ceramic type	Colour	Black core	Techniques used
GRF2	Amphora	Yellow–orange		XRF, PXRD, POM, FESEM, Hydric
GRF6	Vessel	Dark orange	X	XRF, PXRD, POM, FESEM, Hydric
GRF7	Amphora	Dark orange		XRF, PXRD, POM, FESEM, Hydric
GRF11	Amphora	Brown	X	XRF, PXRD, POM, FESEM, Hydric
GRF12	Amphora	Dark yellow	X	XRF, PXRD, POM, FESEM, Hydric, MIP
GRF13	Amphora	Yellow		XRF, PXRD, POM, FESEM, Hydric
GRF15	Amphora	Brown	X	XRF, PXRD, POM, FESEM, Hydric
GRF16	Vessel	Dark orange		XRF, PXRD, MIP
GRF17	Amphora	Yellow–orange	X	XRF, PXRD, POM, FESEM, Hydric, MIP
GRF18	Amphora	Brown	X	XRF, PXRD, Hydric
GRF19	Amphora	Yellow–orange	X	XRF, PXRD, POM, FESEM, Hydric, MIP
GRF20	Amphora	Yellow–orange	X	XRF, PXRD, Hydric
GRF21	Vessel	Brown	X	XRF, PXRD, POM, FESEM, MIP
GRF22	Vessel	Brown	X	XRF, PXRD, POM, FESEM, MIP
GRF23	Amphora	Brown		XRF, PXRD, POM, FESEM, Hydric, MIP
GRF24	Vessel	Dark orange		XRF, PXRD, MIP
GRF25	Vessel	Yellow–orange	X	XRF, PXRD, Hydric
GRF26	Vessel	Yellow–orange		XRF, PXRD, POM, FESEM, Hydric
GRF27	?	Yellow–orange		XRF, PXRD, POM, FESEM, Hydric, MIP
GRF28	Amphora	Pale yellow		XRF, PXRD, POM, FESEM, Hydric, MIP
GRF29	Vessel	Brown		XRF, PXRD, POM, FESEM, MIP
GRF30	Vessel	Brown		XRF, PXRD
GRF31	Vessel	Brown		XRF, PXRD, MIP
GRF32	Vessel	Yellow–orange	X	XRF, PXRD, MIP
GRF33	Vessel	Orange	X	XRF, PXRD, POM, FESEM, MIP
GRF34	Vessel	Yellow–orange		XRF, PXRD, MIP
GRF35	Amphora	Yellow	X	XRF, PXRD, Hydric
GRF36	Amphora	Yellow–orange	X	XRF, PXRD, POM, FESEM, Hydric
GRF37	Amphora	Yellow–orange		XRF, PXRD, Hydric
GRF38	Vessel	Yellow–orange	X	XRF, PXRD, Hydric, MIP
GRF39	Vessel	Yellow–orange	X	XRF, PXRD, POM, FESEM, Hydric
GRF40	Vessel	Orange		XRF, PXRD, POM, FESEM, Hydric, MIP
	Age	**Details of raw materials**		
Raw1	Plio-Pleistocene	Red-brown clay at the settlement, on Canto Tortoso hill		
Raw2	Turolian-Pliocene	Pale grey clay near the settlement, on Canto Tortoso hill		
Raw3	Holocene	Pale brown clay in talus cone near Guadiana Menor River		
Raw4	Holocene	Grey clay in the alluvial fan of Guadiana Menor River		
Raw5	Holocene	Brownish clay in the alluvial fan of Fardes River		
Raw6	Holocene	Dark grey clay in the floodplain of Fardes River (near the kiln)		

with certified values of the analysed reference materials [20]. Typical precision is higher than 1.5% relative to a concentration of 10%. Loss on ignition was determined gravimetrically as the weight loss was recorded between 110 °C and 1000 °C. The De Jongh model [21] was followed to convert the measured intensities to concentrations, using Alpha-coefficients.

The chemical elements in the samples were correlated to the mineral phases determined by means of powder X-ray diffraction (PXRD). A Philips X'Pert Pro diffractometer was used; the working conditions were: CuKα radiation emission ($\lambda = 1.5405$ Å), 45 kV voltage, 40 mA current, 3–70° 2θ explored area and 0.1° $2\theta\ s^{-1}$ goniometer speed. The X-ray diffraction patterns were interpreted using the XPowder© program [22].

The mineralogical study was completed with the observation of mineral sizes and shapes and ceramic textures using a Zeiss Jenapol polarised optical microscope (POM). Images were obtained by means of an Olympus DP-10 microphotography unit.

The microtexture, degree of vitrification and composition of detailed mineral phases were determined using a Leo Gemini 1530 Field Emission Scanning Electron microscope (FESEM) coupled with Oxford Inca 200 EDS microanalysis. FESEM back-scattered electron (BSE) images were obtained using polished carbon-coated thin sections.

Various authors consider a porosity study a valid tool for obtaining information on the firing temperature and the technology used in making ceramics [23–25]. For this purpose, we carried out free and forced water absorption [26] and drying tests [27] in order to determine the influence of the open porosity on the water flow through the ceramic samples. The saturation coefficient, drying index, bulk and real (skeletal) densities and open porosity [28] were calculated. The only

deviation from the EN, Normal and RILEM standard procedures is that we did not have cylindrical- or cubic-shaped samples of 5 cm edge at our disposal, but only irregular fragments of different sizes, shapes and weights. This test was carried out on samples with a dry weight of over 15 g. We determined the porosity and pore size distribution of lighter samples by means of mercury intrusion porosimetry (MIP) using a Micromeritics Autopore III 9410 apparatus, which measures pores with radii of between 0.003 and 360 μm and to exert a maximum pressure of 414 MPa. Two fragments of ~2 cm^3 per sample were oven-dried for 24 h at 100 °C prior to the analysis. The samples with distinctive hydric test results were also chosen for the pore system analysis by MIP.

3. Results and discussions

3.1. XRF

Table 2 shows the chemical composition of ceramics in percentage terms. Samples are rich in SiO_2 with a mean content of 55 wt%, where the richest, GRF7, reaches 70 wt% and the poorest, GRF21, 44 wt%. The second most abundant compound is Al_2O_3 which varies from 13 wt% (GRF21) to 23 wt% (GRF33). GRF21 sample has the highest CaO content (17.5 wt%). Maniatis and Tite [29] proposed that ceramics are classified as non-calcareous or calcareous when the CaO content is less or more of 6 wt% respectively. Using this classification, we identified 17 non-calcareous ceramics (of which GRF22 had the lowest CaO content) and 15 calcareous ceramics. The difference in the amount of CaO can be attributed to various factors, such as the use of different raw materials (rich and poor in carbonates) or the addition of calcite when the potter wanted to produce a piece for certain specific purposes [6,30,31]. Moreover, we cannot discard an enrichment in CaO caused by the circulation of Ca-rich solutions from the ground to the pore system of the ceramics [32]. The samples we studied are also characterised by variable amounts of Fe_2O_3, MgO and K_2O. The GRF23 sample is worthy to mention because it has the highest MgO content, over two times higher (7.7 wt%) than the other samples (0.9–2.8 wt%), the highest K_2O content (4.6 wt%) and the second highest Fe_2O_3 content (8.6 wt%). Despite its CaO content was less than 6 wt%, this sample was also included within the calcareous ceramics in which presumably dolomite prevailed on calcite.

Table 2
Chemical analyses of ceramic samples (in wt%). Ceramics are divided on the basis of CaO content in calcareous (CaO > 6 wt%) and non-calcareous ceramics (CaO < 6 wt%). GRF23 sample is included in calcareous ceramics because of its high MgO content.

	SiO_2	Al_2O_3	Fe_2O_3	MnO	MgO	CaO	Na_2O	K_2O	TiO_2	P_2O_5	LOI
Calcareous ceramics											
GRF6	53.83	18.99	6.94	0.04	2.24	7.52	0.47	3.29	0.79	0.19	5.05
GRF12	52.66	21.87	7.21	0.04	2.33	7.66	0.54	3.68	0.62	0.20	2.70
GRF13	55.15	21.13	6.69	0.04	2.25	6.10	0.56	3.40	0.60	0.14	3.48
GRF17	52.83	18.23	6.30	0.04	2.22	10.37	0.44	3.17	0.57	0.19	5.13
GRF21	43.58	13.32	4.32	0.02	1.83	17.49	0.13	2.28	0.61	0.10	15.66
GRF23	50.53	18.00	8.58	0.10	7.71	5.55	0.56	4.62	1.07	0.19	2.88
GRF25	50.26	20.47	7.31	0.03	2.08	6.68	0.40	3.62	0.58	0.19	7.62
GRF26	59.93	15.78	5.29	0.03	2.41	8.08	0.07	3.99	0.81	0.13	2.86
GRF28	55.51	19.40	6.95	0.04	1.91	8.05	0.41	3.08	0.88	0.17	2.91
GRF32	50.83	19.07	7.07	0.04	2.24	9.35	0.47	3.37	0.66	0.23	6.06
GRF34	57.10	17.39	5.61	0.03	2.57	8.76	0.25	4.10	0.81	0.11	2.89
GRF35	55.42	20.10	6.04	0.04	2.09	6.91	0.58	3.50	0.54	0.17	3.93
GRF36	55.96	19.18	5.84	0.03	1.87	7.92	0.52	3.30	0.73	0.19	3.98
GRF37	54.31	20.92	6.42	0.04	1.88	6.03	0.56	3.68	0.64	0.14	4.94
GRF39	53.12	18.90	6.96	0.04	2.40	8.74	0.49	3.28	0.85	0.22	4.51
GRF40	53.96	18.19	5.94	0.03	2.85	8.54	0.03	4.06	0.89	0.13	4.88
Non-calcareous ceramics											
GRF2	61.29	21.37	6.12	0.03	1.90	1.31	0.60	3.63	0.77	0.09	2.54
GRF7	70.33	14.78	5.74	0.05	0.89	1.04	0.45	2.37	0.98	0.08	2.76
GRF11	60.67	22.28	5.71	0.03	1.64	1.29	0.51	3.72	0.82	0.11	2.70
GRF15	55.10	22.32	7.68	0.03	2.04	3.56	0.64	3.88	0.59	0.16	3.46
GRF16	60.42	20.47	6.05	0.03	2.02	2.06	0.75	3.63	0.75	0.08	3.07
GRF18	54.23	21.82	7.79	0.03	2.07	4.07	0.64	3.85	0.58	0.16	4.09
GRF19	54.29	20.15	7.30	0.04	1.91	5.12	0.50	3.58	0.61	0.19	5.94
GRF20	53.42	18.98	7.07	0.05	2.09	5.94	0.37	3.45	0.66	0.22	7.12
GRF22	64.83	18.19	7.17	0.10	1.31	0.99	0.51	2.75	0.94	0.09	2.51
GRF24	55.74	21.03	7.56	0.04	2.19	5.26	0.60	3.58	0.93	0.17	2.50
GRF27	62.70	20.18	5.81	0.06	1.01	1.05	0.98	3.69	0.86	0.12	3.01
GRF29	59.98	21.05	6.95	0.08	1.35	1.78	0.56	3.24	1.25	0.10	2.89
GRF30	53.88	18.46	7.34	0.06	1.15	5.77	n.d.	3.57	0.69	0.11	8.50
GRF31	57.22	20.72	7.41	0.04	2.43	4.16	0.67	3.62	0.83	0.19	2.05
GRF33	53.34	22.88	8.61	0.03	2.37	4.94	0.58	3.80	0.63	0.20	1.91
GRF38	55.74	21.83	7.42	0.03	2.07	4.36	0.65	3.85	0.69	0.62	2.15

3.2. PXRD

The PXRD results (Table 3) are clearly linked to the chemistry described above. The 32 ceramics are almost all rich in quartz; this phase is indicated as abundant to very abundant in Table 3. The only exception was sample GRF21 where calcite predominates. This carbonate was identified in slightly more than half the samples but generally in scarce or trace concentrations. The other carbonate, dolomite, was detected in very low concentration only in GRF18 and GRF25. The presence of dolomite and calcite, when the latter is not of secondary origin, suggest that ceramics were fired at low temperatures, of around 700–750 °C in an oxidising atmosphere [33] or at a temperature 50 °C higher in a reducing atmosphere and submerging the fired product in cold water [34]. The only phyllosilicate identified is illite which appears in all the samples albeit in moderate amounts. Feldspars *s.l.* were detected in many samples but generally in very low quantities and mainly as K-feldspars and to a lesser extent Ca–Na plagioclases. Low concentrations of haematite and, in some samples, of gehlenite, diopside and mullite were detected. GRF23 stands out when compared to the other ceramics because it has the highest gehlenite and diopside concentrations. The presence of gehlenite, diopside and mullite indicates that the ceramics were fired at a high temperature (>900 °C) [35]. The literature on the mineralogical reactions occurring in ceramics during firing indicates that gehlenite ($Ca_2Al_2SiO_7$) is formed after the decomposition of calcite and the reaction of CaO with dehydroxylated phyllosilicates [36], while diopside ($CaMgSi_2O_6$) develops at the interface between silicates (quartz plus phyllosilicates) and dolomite, which provides Ca and Mg [33] or during firing of calcareous clays containing chlorite [37]. Mullite ($Al_6Si_2O_{13}$) is formed after muscovite breakdown while preserving its structure (epitactic replacement [38]). However, the above reactions do not exclude the possibility of temperature variations of hundreds of degrees inside the kiln, both in pieces fired at the same time and within the same ceramic piece if it is large-sized [14,39]. As regards the firing temperature, we have also considered the presence of an amorphous or vitreous phase detected from the background noise in the X-ray diffraction patterns [40]. The highest noise was detected in the GRF23 sample in which we also observed the highest amount of new silicate phases.

The raw materials were found to have different mineralogy and three of them, Raw1, Raw2 and Raw3, can be discarded as they are too rich in calcite and poor in quartz and clay minerals. This would make them difficult to use in ceramic production and might also lead to lime blowing phenomena after firing. The other three raw materials (Raw4, Raw5 and Raw6) seem to be more suitable for making pottery and their composition is closer to that of our ceramics. They came from the sediments from the Guadiana Menor and Fardes rivers and are rich in phyllosilicates of illitic composition plus smaller amounts of chlorite and paragonite. Raw5 and Raw6 are the most similar to the ceramics, especially the latter, which is the richest in quartz and phyllosilicates and has the lowest carbonate concentration of the six sediments. Notice that Raw6 was the closest to the Iberian Age kiln discovered near the settlement. Raw4 might have been used to make GRF21 because of its higher calcite content. All of the raw materials we studied contain calcite. This might suggest that the ceramics that do not contain this carbonate and/or Ca silicates were made using raw materials from another, more distant, source. However, if we assume that potters almost certainly sourced the raw material nearby, from along the banks of the Fardes River (Raw6), it is logical that the composition of the soil could vary in composition, for example in the amount of carbonates, depending on the flow rate and the sediments transported by the river. This is proved by the mineralogical variations between the Raw4, Raw5 and Raw6 samples collected at relatively short distances from one another.

3.3. POM

The main petrographic features of the ceramics are summarised in Table 4. Quartz is the most common mineral in the ceramic samples and can be observed in isolated crystals or as a constituent of gneiss and micaschist fragments (Fig. 2a). It has an angular shape, undulose extinction and varying size, from a few micrometres to 3–4 mm in the case of gneisses. This is the main component of the ceramic temper, although in some cases we also observed calcite grains measuring a few millimeters-thick. In all the samples there was more quartz than calcite, except for GRF21 where calcite predominates, as shown also by PXRD. In this sample, the typical double exfoliation system and polysynthetic twinning of calcite as well as the high order interference colours under crossed nicols clearly suggest a low firing temperature, below 750 °C (Fig. 2b). The presence of calcite grains angular in shape and irregular in size suggests that they may have been crushed and intentionally added to the mixture for the use of artefact as cooking ceramic [34]. Calcite grains with similar morphology but in lower amount have been also observed in GRF6, GRF17 and GRF36 samples (Table 4). As the firing temperature increases the carbonate turns darker in colour (Fig. 2c). On occasions we also observed plagioclase crystals twinned according to the albite law (Fig. 2d). As can be seen in Fig. 2 and Table 4, the matrix of the ceramics varies from fine to coarse, due to the fact that some pieces have higher temper content. These textural data can provide information as to the purpose of the ceramics (ritual, domestic, for transport). It is likely that the potters added different amounts of temper depending on the particle-size distribution of the raw material to avoid high shrinkage during drying and firing. In addition, a high temper content could reflect the potters' interest in ceramics with high toughness and thermal shock resistance [41], while low temper concentrations would have produced pieces with high strength [34].

Phyllosilicates are mainly of the muscovite-type and in some cases they are aligned due to the pressure exerted by the potter on the raw material during the kneading (Fig. 2e). They have a laminar habit and can be observed as dispersed crystals in the matrix or as components of gneisses and micaschists fragments. The degree of matrix vitrification is indicative of the

Table 3
Mineralogical composition of ceramic samples and raw materials on the basis of PXRD analysis. Qz=quartz; Ilt=illite/muscovite; Cal=calcite; Kfs=K-feldspar; Hem=haematite; Dol=dolomite; Pl=plagioclase; Gh=gehlenite; Di=diopside; Mul=mullite; m=melt; Sme=smectite; Pg=paragonite; Chl=chlorite; Gp=gypsum; × × × × =very abundant; × × × =abundant; × × =moderate; × =scarce; and tr=in traces (mineral symbols after Whitney and Evans [52]).

	Qz	Ilt	Cal	Kfs	Hem	Dol	Pl	Gh	Di	Mul	m
Calcareous ceramics											
GRF6	× × ×	×	×	×	tr						×
GRF12	× × ×	×	×	×	tr		×			×	× ×
GRF13	× × ×	× ×	×	×			tr				×
GRF17	× × ×	×	× ×	×			tr				×
GRF21	× ×	tr	× × ×								×
GRF23	× × ×				×		× ×	× ×	× ×		× × ×
GRF25	× × ×	×	×	×	tr	tr					×
GRF26	× × ×	×					×	×	×		×
GRF28	× × × ×	×			tr		×		×		×
GRF32	× × ×	tr	× ×	×	tr						× ×
GRF34	× × ×	tr	×				×	tr	×		×
GRF35	× × × ×	×	×	×							×
GRF36	× × × ×	×	×				×				×
GRF37	× × × ×	×	×	×						tr	×
GRF39	× × ×	tr	×		tr		×	tr	×		×
GRF40	× × × ×		×				×		×		× ×
Non-calcareous ceramics											
GRF2	× × × ×	×		tr							×
GRF7	× × × ×	× ×									tr
GRF11	× × ×	× ×		×							×
GRF15	× × × ×	×	×	×	tr					×	× ×
GRF16	× × × ×	tr	tr	×							×
GRF18	× × × ×	tr	×	×	tr	tr					×
GRF19	× × × ×	tr	×	×	tr						× ×
GRF20	× × ×	×	×	×	tr						× ×
GRF22	× × × ×	× ×			tr						×
GRF24	× × ×	×	×	×	tr						×
GRF27	× × × ×	×		tr							×
GRF29	× × × ×	×		×	tr						×
GRF30	× × ×	tr	×	×	tr						× ×
GRF31	× × × ×	×			×		tr				× ×
GRF33	× × ×	tr		× ×	×		tr			×	× ×
GRF38	× × × ×	tr			tr		×			×	× ×
	Qz	**Ilt**	**Cal**	**Kfs**	**Hem**	**Dol**	**Pl**	**Sme**	**Pg**	**Chl**	**Gp**
Raw1	×	tr	× × × ×	tr	tr	tr		×			
Raw2	× ×	tr	× × ×	tr		tr		tr			× ×
Raw3	× ×	×	× × × ×	tr		tr					
Raw4	× × ×	× ×	× × ×				×		tr	tr	× ×
Raw5	× × ×	× ×	× × ×	×		×	×			tr	
Raw6	× × × ×	× × ×	× ×				×		×	×	

Table 4
Textural features of ceramics by means of MOP observations. Q, C, M, G and P are, respectively, quartz, calcite, micaschist, gneiss and plagioclase temper fragments; I, E and R refer, respectively, to irregular, elongated and rounded-shaped pores.

	Temper	Texture	Matrix birefringence	Pore shape
Calcareous ceramics				
GRF6	Q, G, C	Coarse	High	I, E
GRF12	Q, G	Fine	Low	E, R
GRF13	Q, G, M	Fine	High	I
GRF17	Q, G, C	Intermediate	High	I
GRF21	C, Q	Coarse	High	E, I
GRF23	Q, P	Coarse	Low	E
GRF26	Q	Fine	Low	R, E
GRF28	Q, G, M	Intermediate	Low	I, E
GRF36	Q, G, C	Intermediate	High	I
GRF39	Q, G, M	Fine	Low	E
GRF40	Q	Fine	Low	I, E
Non-calcareous ceramics				
GRF2		Intermediate	High	E
GRF7	Q, G, M	Coarse	High	I, E
GRF11		Intermediate	High	I, E
GRF15	Q, G	Fine	Low	E
GRF19		Intermediate	Low	E, I
GRF22	Q, G, M	Coarse	High	I, E
GRF27		Coarse	High	I
GRF29	Q, G, M	Intermediate	High	I, E
GRF33	Q, G	Fine	Low	R, E

firing temperature: low-fired samples are more birefringent than high-fired ones. This occurred in half of the samples observed by POM (Table 4).

Among accessory minerals, epidote and Fe-oxides are the most common but graphite and metal ores were also observed.

The pores differ in terms of size and shape, the latter varying generally from irregular vughs to elongated, and sometimes also rounded. In some cases, the edges of the pores are coated by a thin micritic calcite fringe of secondary origin, precipitated from Ca-rich solutions circulating in the ground where the ceramics were buried (Fig. 2f). This explains the presence of this carbonate in GRF12, GRF34, GRF39 and GRF40, as detected by PXRD together with mullite, gehlenite and/or diopside (see Table 3), which formed at high temperatures. Calcite of secondary origin has also been found covering the surface of some ceramics as an irregular layer about 200 μm thick, which forms the white patina described above.

3.4. FESEM+EDS

This technique was very helpful when observing the microtexture of ceramics and the presence of new minerals grew during firing at certain temperatures and for identifying the presence of various scarce phases which passed unnoticed under PXRD and POM. The observation of ceramics at low magnification confirms the abundance of quartz grains and the two types of matrices, coarse and fine (Fig. 3a and b). FESEM images highlight the presence of fissures at grain boundaries in samples with a coarse matrix (Fig. 3a). Kilikoglou et al. [42] argued that these fissures were the result of the shrinkage of clay minerals during drying and the expansion of quartz crystals during firing (from α phase to polymorph β), a beneficial phenomenon in that it increases the toughness of the ceramics. Besides the minerals already identified by PXRD, small bright ilmenite and rutile crystals were also observed in almost all samples.

A general view of the GRF21 sample confirms that, unlike the other samples, the temper used in this vessel is mainly composed of calcite grains (Fig. 3c). In this ceramic, the calcite has an angular shape and cleavage surfaces are visible. However, higher magnification of the calcite crystals revealed that there are nanometric pores along these planes. These pores were presumably generated by the incipient decomposition of carbonate and the release of CO_2 (Fig. 3d). Therefore, even if calcite appears unchanged under an optical microscope (see Fig. 2b), the firing temperature is high enough to start damaging its crystal structure. On this question, Rodriguez Navarro et al. [43] observed that the initial thermal decomposition of calcite is accompanied by the development of nanopores inside the crystals. However, we did not detect any new silicate phases along the edges of the calcite grains (i.e. no reaction with silicates started) denoting the low firing temperature of this ceramic.

In Ca-rich ceramics fired at higher temperatures, bright reaction rims developed between decomposed carbonates and silicates (quartz plus phyllosilicates). New silicates, such as gehlenite and diopside formed (Fig. 3e), and plagioclase turned anorthitic in composition.

As regards muscovite, low fired samples show the typical laminar habit of unaltered mica, although the crystals show a marked basal exfoliation due to dehydroxylation (Fig. 3f). In ceramics fired at high temperatures, muscovite lost its habit and developed a secondary porosity indicating extensive melting (Fig. 3g). Some melted muscovite crystals maintained

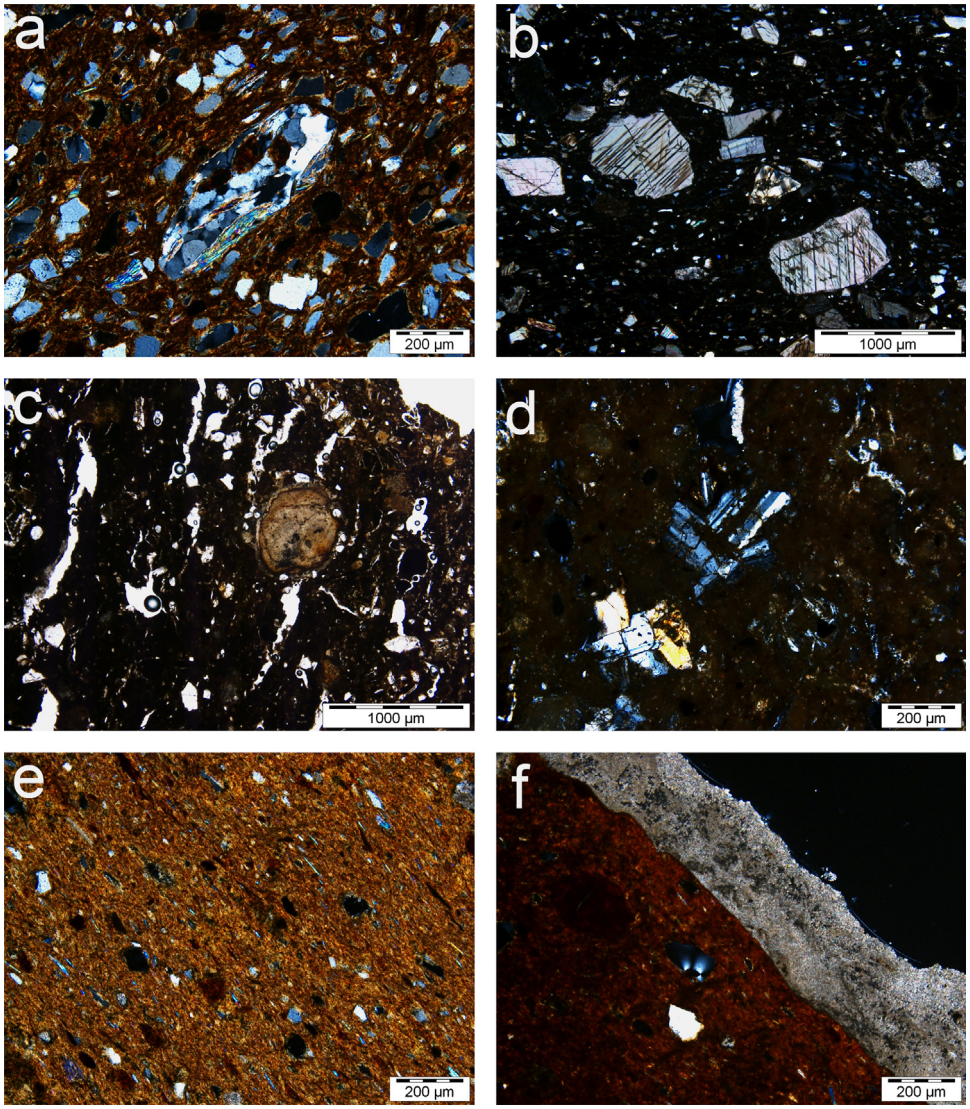

Fig. 2. Optical microscopy images of (a) quartz fragments with undulose extinction and a gneiss fragment with birefringent muscovite crystals in sample GRF7 with coarse matrix (cross-polarised light); (b) twinned and exfoliated calcite crystals with angular morphology in sample GRF21 (cross-polarised light); (c) dark calcite grain in high-fired sample GRF23 (plane-polarised light); (d) plagioclase crystals twinned according to the albite law in sample GRF23 (cross-polarised light); (e) small birefringent muscovite crystals aligned in a fine matrix in sample GRF15 (cross-polarised light); and (f) irregular calcite layer of secondary origin covering the surface of sample GRF33 (cross-polarised light).

a relatively intact core (Fig. 3g). A detailed image reveals the presence of nanometric bright mullite crystals embedded in part of the melted crystal (Fig. 3h), thus confirming PXRD analysis (Table 3). The development of mullite from rich muscovite materials under high firing temperatures has been described by several authors in peraluminous rocks that had suffered pyrometamorphism [35,44,45] and in ceramics [38,46,47]. The mullite composition is very similar to that of muscovite but with a higher Al content (see the insets spectrum in Fig. 3h). It is interesting that mullite is distributed on the melted edges (comparable to "mullite buchites" of peraluminous xenoliths [48]) and not in the still preserved core of the crystals.

High magnification images allowed us to distinguish the degree of vitrification reached by the matrix. Low fired samples have angular pores that were produced during the moulding of the pieces and there is limited interlocking between particles (Fig. 3f). In samples fired at higher temperature a new type of pore with spherical and ellipsoidal morphology appear, as a result of the melting of clay minerals in the matrix and the release of gas [49] (Fig. 3g).

3.5. Hydric tests

The first thing we noted is that the CaO content has no influence on the hydric behaviour of ceramics (Table 5). Free water absorption (A_b) varies from 10–11% to 19–21% in both calcareous and non-calcareous samples. These values suggest that the ceramics we studied have quite high compactness when compared with similar products [6,25,50,51]. There is no great difference between free (A_b) and forced water absorption (A_f), which means a relatively good pore interconnection.

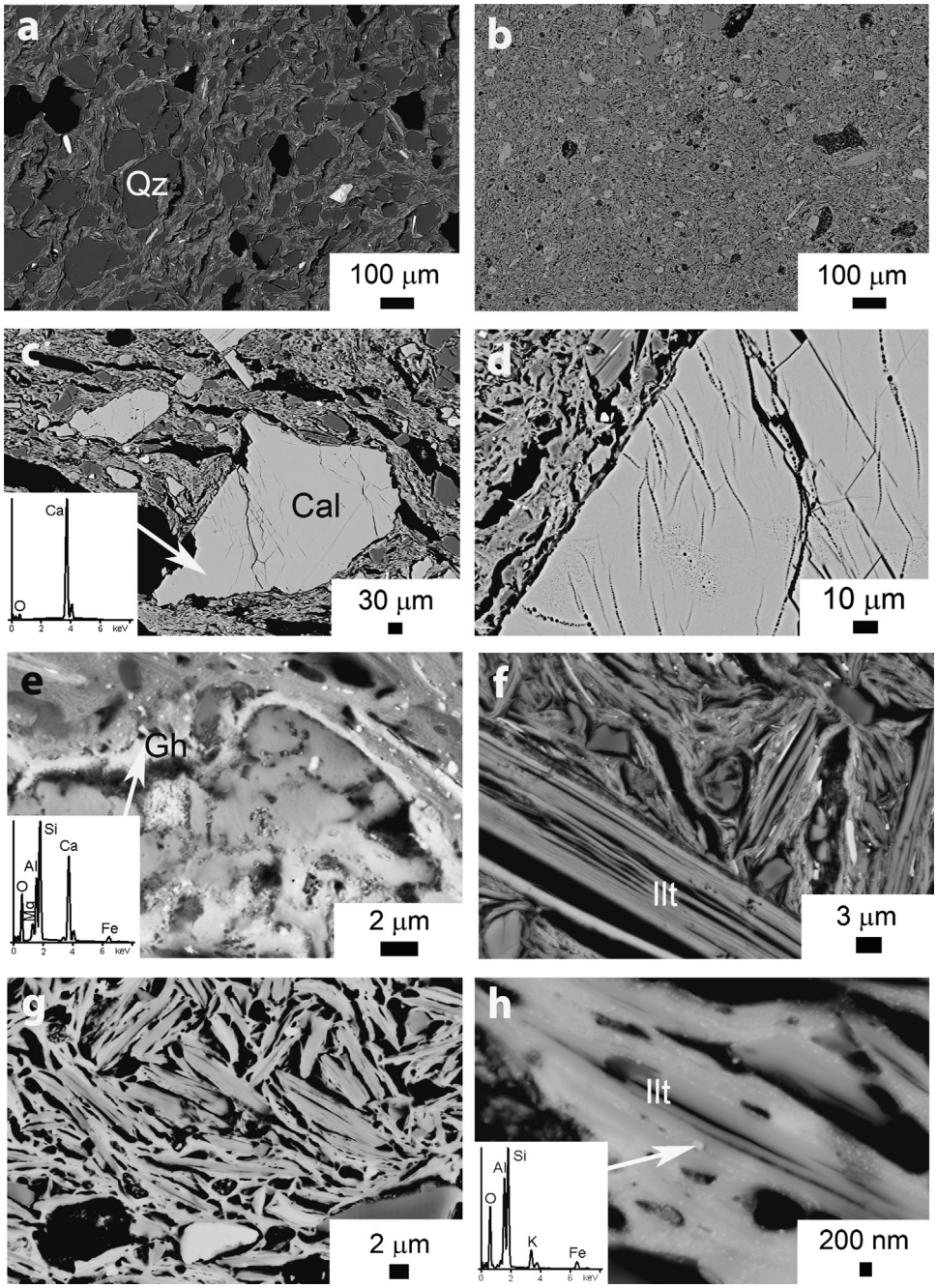

Fig. 3. BSE images and EDS analyses of ceramic samples: (a) general view of GRF7 sample showing a coarse texture with fissures at quartz grain boundaries (Qz); (b) general view of GRF26 sample showing a fine texture; (c) general view of low-fired GRF21 ceramic in which the abundance of calcite crystals (Cal) with angular morphology and double exfoliation system are visible (see spectrum); (d) detailed image of a calcite crystal that shows the development of nanopores along weakness lines; (e) development of a bright reaction rim around a former calcite crystal that is composed of gehlenite (Gh) (see spectrum) in a high-fired GRF23 sample; (f) typical habit of phyllosilicate crystals (Ilt) showing separation along the basal planes in the GRF7 sample; (g) partially melted phyllosilicate crystals in the high-fired GRF33 sample. Primary porosity is easily distinguishable from more rounded secondary porosity; and (h) detailed image of a phyllosilicate in the same sample showing that melting develops from the outside to the inside of the still-preserved crystal (Ilt). Extensive nanometric bright mullite crystals were growing in the melted phyllosilicate (see spectrum).

Indeed, the saturation coefficient (S) is around 90% or higher. The only exception is GRF23, which has an S value of 69%. The samples that absorb less water tend to dry slowly (higher Di values). This is because they are more compact, as can be deduced by their higher apparent density values (ρ_b), which are slightly different from those for skeletal density (ρ_{sk}), i.e. there are less empty spaces in these ceramics. This is the case of GRF17, GRF36 and GRF39 in the group of calcareous ceramics and of GRF7, GRF11 and GRF23 in non-calcareous ceramics (Table 5). On the contrary, the samples that absorb more water, such as GRF38 and GRF40, are characterised by a low ρ_a and the highest open porosity (Po around 34%). It is worth remembering

Table 5
Hydric parameters of calcareous and non-calcareous ceramics. A_b=free water absorption (%); A_f=forced water absorption; S=saturation coefficient (%); Di=drying index; ρ_b=apparent density (g/cm^3); ρ_{sk}=skeletal (real) density (g/cm^3); Po=open porosity (%); SSA=specific surface area (m^2/g, determined by MIP); and Po_{MIP}=open porosity (%, determined by MIP).

	A_b	A_f	S	Di	ρ_b	ρ_{sk}	Po	SSA	Po_{MIP}
Calcareous ceramics									
GRF6	15.96	16.85	89.70	0.916	1.75	2.48	29.43		
GRF12	16.06	16.31	93.08	0.921	1.77	2.49	28.87	5.08	31.16
GRF13	18.59	19.35	92.53	0.911	1.72	2.58	33.33		
GRF17	11.54	11.89	93.00	0.940	1.86	2.39	22.15	5.02	28.15
GRF21								6.36	20.06
GRF23	10.12	12.32	69.09	0.935	2.00	2.65	24.61	6.08	24.44
GRF25	16.34	16.62	96.47	0.926	1.79	2.54	29.71		
GRF26	14.89	14.99	89.67	0.924	1.83	2.51	27.37		
GRF28	18.75	19.27	93.41	0.915	1.74	2.61	33.44	8.36	33.62
GRF32								5.96	29.17
GRF34								4.44	32.20
GRF35	14.10	14.62	90.39	0.926	1.81	2.47	26.53		
GRF36	12.18	12.42	95.94	0.938	1.85	2.40	22.94		
GRF37	16.24	16.58	94.49	0.923	1.76	2.48	29.17		
GRF39	12.95	13.24	94.37	0.933	1.85	2.46	24.55		
GRF40	20.88	21.41	90.08	0.906	1.63	2.50	34.91	6.41	34.68
Non-calcareous ceramics									
GRF2	15.35	15.59	94.12	0.926	1.79	2.48	27.87		
GRF7	10.97	11.39	91.40	0.939	1.96	2.53	22.37		
GRF11	11.72	11.83	95.76	0.936	1.93	2.50	22.83		
GRF15	17.19	17.95	91.60	0.916	1.74	2.53	31.22		
GRF16								7.89	31.32
GRF18	17.68	18.06	94.15	0.920	1.75	2.55	31.55		
GRF19	17.81	18.03	95.29	0.920	1.74	2.53	31.36	10.42	27.35
GRF20	16.51	17.09	93.83	0.924	1.80	2.59	30.69		
GRF22								7.12	23.04
GRF24								3.22	29.84
GRF27	15.67	16.87	87.33	0.919	1.82	2.62	30.62	5.58	29.13
GRF29								5.23	24.46
GRF31								2.54	27.72
GRF33								6.48	30.59
GRF38	19.54	20.28	89.08	0.908	1.68	2.54	34.03	2.27	34.59

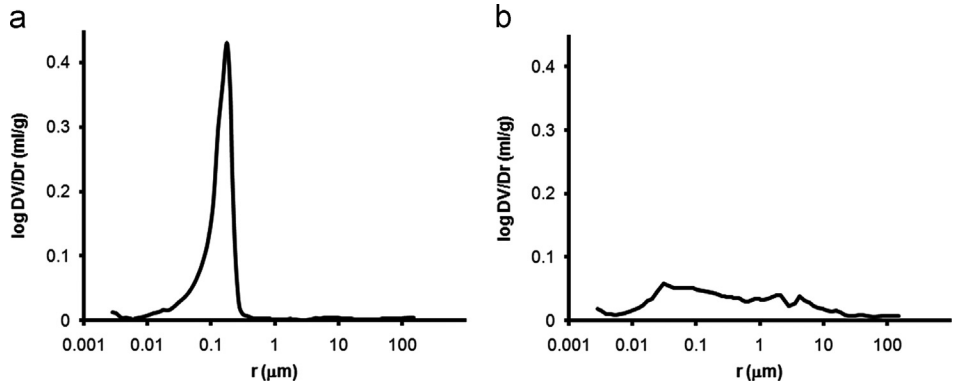

Fig. 4. MIP pore-size distribution curves (log differential intruded volume, in ml g^{-1}, versus pore radius, in μm) of GRF12 (a) and GRF23 (b) samples.

that the porosity values obtained may not reflect the original porosity of the ceramics since after many centuries buried in the soil, the pore system could have changed due to the crystallisation of phases of secondary origin in the empty spaces (as observed under the microscope, see Fig. 2) or leaching processes which may have created new pores [51]. This is why, contrary to what one might have expected, samples with a high degree of vitrification and a fine texture, such as for example GRF40, show a higher porosity and lower apparent density values than less vitrified samples with a coarser texture, such as GRF17.

3.6. MIP

We have noticed that the type of matrix, coarse or fine, identified by POM and FESEM, is by far the most important

Table 6
Summary of chemical, mineralogical, textural and physical characteristics of Iberian ceramics from Canto Tortoso. The firing temperature (°C), in oxidising atmosphere, has been estimated on the basis of distinctive factors extrapolated from the techniques we used. Legend: Ilt = illite/muscovite; Cal = calcite; Dol = dolomite; Kfs = K-feldspar; Pl = plagioclase; Gh = gehlenite; Di = diopside; Mul = mullite; and m = melt (mineral symbols after Whitney and Evans [52]). Estimated firing temperature legend: $A = \leq 750$ °C; $B = 751–850$ °C; $C = 851–950$ °C; and $D = > 950$ °C.

	Type	Colour	XRF	PXRD	POM + FESEM		Hydric tests + MIP		Estimated firing temperature
			CaO content [a]	*Mineralogy*	*Type of texture*	*Vitrification degree*	*Porosity (%)*	*Porometric curve*	
GRF6	Vessel	Dark orange	> 6 wt%	Ilt, Cal, Kfs	Coarse	Low	29		B
GRF12	Amphora	Dark yellow		Mul, **m**	Fine	High	29	Unimodal	D
GRF13	Amphora	Yellow		**Ilt**, Cal, Kfs	Fine	Low	33		B
GRF17	Amphora	Yellow–orange		Ilt, Cal, Kfs	Intermediate	Low	22	Unimodal	B
GRF21	Vessel	Brown		**Cal**	Coarse	Low		Polymodal	A
GRF23	Amphora	Brown		Pl, Gh, Di, **m**	Coarse	High	25	POLYMODAL	D
GRF25	Vessel	Yellow–orange		Cal, Dol			30		A
GRF26	Vessel	Yellow–orange		Gh, Di	Fine	High	27		D
GRF28	Amphora	Pale yellow		Pl, Di	Intermediate	Medium	33	Unimodal	C
GRF32	Vessel	Yellow–orange		Cal, **m**				Polymodal	C
GRF34	Vessel	Yellow–orange		Pl, Di				Unimodal	C
GRF35	Amphora	Yellow		Ilt, Cal, Kfs			27		B
GRF36	Amphora	Yellow–orange		Ilt, Cal, Pl	Intermediate	Medium	23		B
GRF37	Amphora	Yellow–orange		Ilt, Mul			29		C
GRF39	Vessel	Yellow–orange		Pl, Di	Fine	High	25		D
GRF40	Vessel	Orange		Di, **m**	Fine	High	35	Unimodal	D
GRF2	Amphora	Yellow–orange	< 6 wt%	Ilt, Kfs	Intermediate	Low	28		B
GRF7	Amphora	Dark orange		**Ilt**	Coarse	Low	22		A
GRF11	Amphora	Brown		**Ilt**, Kfs	Intermediate	Low	23		B
GRF15	Amphora	brown		Mul, **m**	Fine	High	31		D
GRF16	Vessel	Dark orange		Kfs				Polymodal	C
GRF18	Amphora	Brown		Kfs, Dol			32		A
GRF19	Amphora	Yellow–orange		Kfs, **m**	Intermediate	Medium	31	Unimodal	C
GRF20	Amphora	Yellow–orange		Kfs, **m**			31		C
GRF22	Vessel	Brown		**Ilt**	Coarse	Low		Polymodal	B
GRF24	Vessel	Dark orange		Ilt, Kfs				Unimodal	B
GRF27	?	Yellow–orange		Ilt	Coarse	Low	31	Polymodal	B
GRF29	Vessel	Brown		Ilt, Kfs	Intermediate	Low		Unimodal	B
GRF30	Vessel	Brown		Kfs, **m**					C
GRF31	Vessel	Brown		Kfs, **m**				Unimodal	C
GRF33	Vessel	Orange		Kfs, Mul, **m**	Fine	High		Unimodal	D
GRF38	Vessel	Yellow–orange		Pl, Mul, **m**			34	Unimodal	D

XRF: X-ray fluorescence; PXRD: powder X-ray diffraction (bold letters stand for high content); POM: polarised optical microscopy; FESEM: Field Emission Scanning Electron Microscopy; and MIP: mercury intrusion porosimetry.

[a] In GRF23 CaO is less than 6 wt% but MgO is more than 6 wt%.

factor influencing the size and distribution of the pores we have obtained by MIP. In fact, samples with a fine to intermediate texture have a well-defined unimodal pore size distribution and the main peak of pores have a radius comprised between 0.2 and 0.4 μm (Fig. 4a). Whereas, samples with a coarse texture present a polymodal curve with one peak centred at 0.03 and a second, less marked, at 4.2 μm (Fig. 4b). The total correspondence between the type of texture observed under POM and the pore size distribution obtained by MIP allows us to predict whether the texture of a ceramic is coarse or fine just by analysing the porometric curve when it is impossible to prepare thin sections, as happened with some of the samples in this paper. Porosity values (Po_{MIP}, Table 5) are similar to those obtained by hydric tests and range from 20% to 34%, with both analyses showing comparable results in most samples. The specific surface area (SSA) varies from 2 to 10 m^2/g. The increase in SSA is linked to an increase in the number of small pores.

4. Conclusions

Table 6 summarises the main chemical, petrographic and physical differences between Iberian ceramics from Canto Tortoso and details their technological features. As can be seen, XRF and PXRD were the only techniques we were able to use on all the samples. However, the results obtained by combining these techniques with POM, FESEM, hydric tests and MIP allow us to conclude that temperatures of 800–900 °C were reached in most samples. The firing temperature of the studied ceramics was estimated by assessing the decomposition of carbonates and phyllosilicates, the presence of new silicate phases such as gehlenite, diopside, anorthite and mullite and the vitrification of the matrix.

As regards low fired samples, it is important to note that the only ceramic made with large amounts of calcite grains was intentionally fired at low temperatures (around 700–750 °C) due to the risk of lime blowing. This confirms that the potters had acquired a significant degree of technical skill and had some knowledge of the nature of the raw materials they were using and the maximum firing temperatures likely to be reached without breaking the pieces. Moreover, coarse calcite grains were probably added with the precise aim to use the artefacts as cooking ceramics.

A fine texture produces a unimodal pore size distribution curve, while a coarse one gives a polymodal pore network. The perfect match between the results obtained with the porometric study and those from microscope observation provides an insight into the purpose of the ceramic products depending on their finish and the degree of strength or toughness they would have reached on the basis of temper content.

We also found that the composition, texture and firing temperature of the ceramics were the same regardless of their type (amphorae and vessels), with the exception of those ceramics that contain coarse calcite grains.

The contact with the soil favoured the circulation of fluids and the precipitation of calcite forming thin layers on the surfaces as well as inside, in the empty spaces, and this modified, at least partially, the pore system and homogenised the colour of the samples. However, the calcareous ceramics (those with CaO content above 6 wt%) are mainly yellow–orange, whilst the non-calcareous ones (in which the CaO content is under 6 wt%) mainly present a brown colour.

Hydric tests reveal that the carbonate content has no influence on the absorption and drying behaviour of ceramics. In addition, the results obtained with this test sometimes contradict the observations regarding texture (i.e. low-fired ceramics are less porous than high-fired ones). This is because of the exposure to deposition or, on the contrary, leaching processes under burial condition, which may have modified the porosity of the ceramics (filling the pores with secondary phases and/or the formation of new pores due to the decomposition of some minerals). This means that the use of this technique to predict the firing temperature of archaeological ceramics, without the support of other analytical techniques, may lead to erroneous interpretations.

The mineralogical and textural features of the archaeological ceramics suggest that the raw material was of local provenance. The raw material collected along the banks of the Fardes River, near a kiln located 3 km away from the settlement (the kiln and the settlement were coeval) is likely to have been used for making the ceramics. This is the conclusion we reached after comparing six raw materials collected in and around the settlement. It is important to note that the sediments along the river bank have varying composition and that raw materials with different concentrations in carbonates (and some without carbonates) could have been collected. This indicates that the potters knew a lot about the resources available in the area, a fact already observed in Basti, the main settlement of Bastetania [6].

This research has also verified that a valid, reliable interpretation of the origin and the manufacturing process of ancient ceramics can only be obtained by combining and comparing the information obtained from a range of different analytical techniques.

Acknowledgements

This study has been financially supported by Research Group RNM179 of the Junta de Andalucía, by Research Project MAT2012-34473 and by ICON-CICOP Institute of Granada. We are grateful to Alejandro Caballero and the Centro de Estudios Arqueológicos Bastetanos for providing the ceramics. We thank N. Walkington for the translation of the manuscript.

References

[1] D. Parras, P. Vandenabeele, A. Sánchez, M. Montejo, L. Moens, N. Ramos, Micro-Raman spectroscopy of decorated pottery from the Iberian archaeological site of Puente Tablas (Jaén, Spain, 7th–4th century B.C.), J. Raman Spectrosc. 41 (2010) 68–73.

[2] C. González Román, A.M. Adroher Auroux, A. López Marcos, El yacimiento de Canto Tortoso (Gorafe, Granada): un enclave comercial del siglo VI a.C. en el Guadiana Menor, Verdolay: Rev. Mus. Arqueol. Murcia 7 (1995) 159–176.

[3] A.M. Adroher Auroux, La Bastetania arqueológica. Estado de la cuestión, in: A.M. Adroher Auroux, J. Blánquez Pérez (Eds.), Actas del I Congreso Internacional de Arqueología Ibérica Bastetana, Serie Varia 9, Madrid, Spain, 2008, pp. 211–246.
[4] A.M. Adroher Auroux, A. López Marcos, Excavaciones arqueológicas en el Albaicín (Granada). I. El callejón del Gallo, Agencia Patrimonio Albaicín—Granada, Granada, 2001.
[5] J. Barrios Neira, J.L. Lopez Palomo, L. Montealegre Contreras, Caracterización mineralógica y petroestructural de cerámicas protohistóricas, Bol. Soc. Esp. Ceram. Vidr. 33 (1994) 33–40.
[6] G. Cultrone, E. Molina, C. Grifa, E. Sebastián, Iberian ceramic production from Basti (Baza, Spain): first geochemical, mineralogical and textural characterisation, Archaeometry 53 (2011) 340–363.
[7] A.M. Barrachina Ibáñez, Estudio analítico de un conjunto de pastas cerámicas del yacimiento del Pic dels Corbs (Sagunto, Valencia), Cuad. Prehist. Arqueol. Castelló 19 (1998) 153–170.
[8] F. Fernandes, M.M. Jordán, J.D. Martín, T. Sanfeliu, G. Clausell, Estudio arqueométrico de cerámicas ibéricas del yacimiento del Torrelló de Almassora (Castellón), Cesaraugusta 73 (1998) 99–107.
[9] P. López Arce, A. Zornoza Indart, L. Gomez Villalba, E.M. Pérez Monserrat, M. Alvarez de Buergo, G. Vivar, R. Fort, Archaeological ceramic amphorae from under water marine environments: influence of firing temperature on salt crystallisation decay, J. Eur. Ceram. Soc. 33 (2013) 2031–2042.
[10] T. Tortosa, J.M. Rincón, Análisis arqueométrico de cerámicas ibéricas del sureste de la Península Ibérica, Bol. Soc. Esp. Mineral. 20A (1997) 145–146.
[11] C.P. Odriozola, V.M. Hurtado Pérez, The manufacturing process of 3rd millennium BC bone based incrusted pottery decoration from the Middle Guadiana river basin (Badajoz, Spain), J. Archaeol. Sci. 34 (2007) 1794–1803.
[12] M.D. Petit Domínguez, R. García Giménez, M.I. Rucandio, Chemical characterisation of Iberian amphorae and tannin determination as indicative of amphora contents, Microchim. Acta 141 (2003) 63–68.
[13] M.J. Prudêncio, Ceramic in ancient societies: a role for nuclear methods of analysis, in: A.N. Koskinen (Ed.), Nuclear Chemistry: New Research, Nova Science Publishers Inc., New York, 2008, pp. 51–81.
[14] M. Maggetti, C. Neururer, D. Ramseyer, Temperature evolution inside a pot during experimental surface (bonfire) firing, Appl. Clay Sci. 53 (2011) 500–508.
[15] J. Cerdeño del Castillo, R. Díaz Rubio, J. Obis Sánchez, A. Pérez Lorenzo, J. Velasco Vélez, Manual de patologías de las piezas cerámicas para la construcción, AITEMIN, Toledo, 2000.
[16] S. Pavía, The determination of brick provenance and technology using analytical techniques from the physical sciences, Archaeometry 48 (2006) 201–218.
[17] L. Maritan, L. Nodari, C. Mazzoli, A. Milano, U. Russo, Influence of firing conditions on ceramic products: experimental study on clay rich in organic matter, Appl. Clay Sci. 31 (2006) 1–15.
[18] M.S. Tite, Ceramic production, provenance and use. A review, Archaeometry 50 (2008) 216–231.
[19] L. Gredmayer, C.J. Banks, R.B. Pearce, Calcium and sulphur distribution in fired clay bricks in the presence of a black reduction core using micro X-ray fluorescence mapping, Constr. Build. Mater. 25 (2011) 4477–4486.
[20] K. Govindaraju, Compilation of working values and sample description for 383 geostandards, Geostand. Newsl. 18 (1994) 1–158.
[21] W.K. De Jongh, X-ray fluorescence analysis applying theoretical matrix corrections. Stainless steel, X-Ray Spectrom. 2 (1973) 151–158.
[22] J.D. Martín, XPowder, a software package for powder X-ray diffraction analysis, Legal Deposit GR 1001/04, 2004.
[23] S. Freyburg, A. Schwarz, Influence of the clay type on the pore of structural ceramics, J. Eur. Ceram. Soc. 27 (2007) 1727–1733.
[24] A. Mohamed Musthafa, K. Janaki, G. Velraj, Microscopy, porosimetry and chemical analysis to estimate the firing temperature of some archaeological pottery shreds from India, Microchem. J. 95 (2010) 311–314.
[25] G. Velraj, R. Rayma, R. Hemamalini, FT-IR spectroscopy, scanning electron microscopy and porosity measurements to determine the firing temperature of ancient megalithic period potteries excavated at Adichanallur in Tamilnadu, South India, J. Mol. Struct. 1028 (2012) 16–21.
[26] EN 13755. Metodi di prova per pietre naturali. Determinazione dell'assorbimento d'acqua a pressione atmosferica, CNR-ICR, Rome, 2008.
[27] Normal 29/88, Misura dell'indice di asciugamento (Drying Index), CNR-ICR, Rome, 1988.
[28] RILEM, Recommended tests to measure the deterioration of stone and to assess the effectiveness of treatment methods, Mater. Struct. 13 (1980) 175–253.
[29] Y. Maniatis, M.S. Tite, Technological examination of Neolithic-Bronze Age pottery from central and southeast Europe and from the Near East, J. Archaeol. Sci. 8 (1981) 59–76.
[30] R.J. Hoard, M.J. O'Brien, M. Ghazavy Khorasgany, V.S. Gopalaratnam, A material-science approach to understanding limestone-tempered pottery from the Midwestern United States, J. Archaeol. Sci. 22 (1995) 823–832.
[31] N.S. Müller, V. Kilikoglou, P.M. Day, G. Vekinis, The influence of temper shape on the mechanical properties of archaeological ceramics, J. Eur. Ceram. Soc. 30 (2010) 2457–2465.
[32] J. Buxeda i Garrigós, V. Kilikoglou, P.M. Day, Chemical and mineralogical alteration of ceramics from the Late Bronze Age kiln at Kommos, Crete: the effect on the formation of a reference group, Archaeometry 43 (2001) 349–371.
[33] G. Cultrone, C. Rodríguez Navarro, E. Sebastián, O. Cazalla, M.J. De la Torre, Carbonate and silicate phase reactions during ceramic firing, Eur. J. Mineral. 13 (2001) 621–634.
[34] M.S. Tite, V. Kilikoglou, G. Vekinis, Strength, toughness and thermal shock resistance of ancient ceramics, and their influence on technological choice, Archaeometry 43 (2001) 301–324.
[35] R. Grapes, Pyrometamorphism, Springer, Berlin, 2006.
[36] A. Issi, A. Kara, A.O. Alp, An investigation of Hellenistic period pottery production technology from Harabebezikan/Turkey, Ceram. Int. 37 (2011) 2575–2582.
[37] F. Pardo, S. Meseguer, M.M. Jordán, T. Sanfeliu, I. González, Firing transformations of Chilean clays for the manufacture of ceramic tile bodies, Appl. Clay Sci. 51 (2011) 147–150.
[38] C. Rodriguez Navarro, G. Cultrone, A. Sanchez Navas, E. Sebastian, TEM study of mullite growth after muscovite breakdown, Am. Mineral. 88 (2003) 713–724.
[39] M.S. Tite, Firing temperature. How and why? in: A. Lindhal, O. Stilborg (Eds.), KVHAA Konferenser 34: The Aim of Laboratory Analysis in Archaeology, Stockholm, Sweden, 1995, pp. 37–42.
[40] J. Huertas, F. Huertas, J. Linares, Evolución de las fases no cristalinas en cerámicas arqueológicas por DRX, Bol. Soc. Esp. Mineral. 14 (1991) 71–78.
[41] A. De Bonis, C. Grifa, G. Cultrone, P. De Vita, A. Langella, V. Morra, Raw materials for archaeological pottery from the Campania region of Italy: a petrophysical characterisation, Geoarchaeology 28 (2013) 478–503.
[42] V. Kilikoglou, G. Vekinis, Y. Maniatis, P.M. Day, Mechanical performance of quartz-tempered ceramics: Part I, Strength and toughness, Archaeometry 40 (1998) 261–279.
[43] C. Rodriguez Navarro, E. Ruiz Agudo, A. Luque, A.B. Rodriguez Navarro, M. Ortega Huertas, Thermal decomposition of calcite: mechanisms of formation and textural evolution of CaO nanocrystals, Am. Mineral. 94 (2009) 578–593.
[44] M. Hajjaji, A. Belkabir, S.H. Berrada, Peraluminous rocks of Bou-Azzer region (Morocco): geology and firing transformations, J. Afr. Earth Sci. 52 (2008) 114–120.
[45] A.J. Brearley, An electron optical study of muscovite breakdown in pelitic xenolith during pyrometamorphism, Mineral. Mag. 357 (1986) 385–397.
[46] K. Boussois, S. Deniel, N. Tessier-Doyen, D. Chateigner, C. Dublanche-Tixier, P. Blanchart, Characterisation of textured ceramics containing mullite from phyllosilicates, Ceram. Int. 39 (2013) 5327–5333.
[47] R.J. Preston, T.J. Dempster, B.R. Bell, G. Rogers, The petrology of mullite-bearing peraluminous xenoliths: implications for contamination processes in basaltic magmas, J. Petrol. 40 (1999) 549–573.
[48] A. Cairo, B. Messiga, M.P. Riccardi, Technological features of Cotto Variegato: a petrological approach, J. Cult. Herit. 2 (2001) 133–142.

[49] R.M. Esbert, J. Ordaz, F.J. Alonso, M. Montoto, Manual de diagnosis y tratamiento de materiales pétreos y cerámicos, Col.legi d'Aparelladors i arquitectes Tècnics de Barcelona, Barcelona, 1997.
[50] K.G. Harry, A. Johnson, A non-destructive technique for measuring ceramic porosity using liquid nitrogen, J. Archaeol. Sci. 31 (2004) 1567–1575.
[51] F.J. Roldán García, M. Villalobos Megía, E. Lupiani Moreno, J. Hidalgo Ruiz, J. Fernández-Gianotti, Mapa Geológico de España. E. 1:50.000. Hoja 971, Cuevas del Campo, IGME, Madrid, 2009.
[52] D.L. Whitney, B.W. Evans, Abbreviations for names of rock-forming minerals, Am. Mineral. 95 (2010) 185–187.